



Ordered and disordered phases in CaCu₅-type derived structures: Dumbbell cluster modeling with first-principles calculations

Fumiaki Kuroda ^{1,2,*}, Taro Fukazawa,¹ and Takashi Miyake ^{1,2}

¹CD-FMat, National Institute of Advanced Industrial Science and Technology, Tsukuba, Ibaraki 305-8568, Japan

²ESICMM, National Institute for Materials Science, 1-2-1 Sengen, Tsukuba, Ibaraki 305-0047, Japan



(Received 22 June 2021; accepted 12 October 2021; published 7 December 2021)

We investigate the structural stabilities of CaCu₅-type derived structures (Sm_{*m-n*}T_{*5m+2n*}, *T* = Fe, Co) and predict metastable structures with the dumbbell cluster expansion model in which the dumbbell atoms are regarded as virtual single atoms. The metastable structures are concentrated from *n/m* = 1/3 to 1/2, suggesting the existence of compounds with high magnetization. The disordered TbCu₇-type structures are stabilized by the configurational entropy of the dumbbell clusters. The estimated solubility limits of the *T-T* dumbbell are close to the experimental results. The difference in the phase diagram for the Sm-Fe and Sm-Co systems is explained from their effective cluster interactions.

DOI: [10.1103/PhysRevMaterials.5.124405](https://doi.org/10.1103/PhysRevMaterials.5.124405)

I. INTRODUCTION

The development of high-performance magnets is one of the most challenging problems in materials science. These magnets require a ferromagnet with high magnetization, high magnetic anisotropy, and high Curie temperature as the main phase. Compounds containing 3*d* transition metals and rare-earth elements are expected to be good candidates for the main phase, in which the rare-earth elements and 3*d* transition metals are crucial in enhancing the magnetic anisotropy and magnetization, respectively. For example, Nd₂Fe₁₄B is the main phase in NdFeB magnets [1]. However, because Nd₂Fe₁₄B does not have a high Curie temperature (585 K), the development of other permanent magnets is still desirable. Many Fe/Co-rich rare earth compounds have CaCu₅-type derived structures, and most rare-earth magnets to date, with the exception of NdFeB magnets, have this class of compound as the main phase [2].

Rare-earth magnets are classified into structure groups depending on their chemical composition (see Fig. 1 for the schematic crystal structures and Fig. S.1 of the Supplemental Material [3] for details). The simplest group is the CaCu₅-type structure (space group *P6/mmm*), and first-generation rare-earth magnets SmCo₅ and YCo₅ belong to this group [4]. Although SmFe₅ is metastable and does not exist in the Sm-Fe equilibrium phase diagram, it was synthesized using the melt-spinning technique [5]. By replacing *n* out of *m* *R* atoms with a pair of transition metal atoms, known as the *T-T* dumbbell, R_{*m-n*}T_{*5m+2n*} is obtained, where

R is a rare-earth element and *T* is a magnetic transition-metal element. For [(*m*, *n*) = (3, 1)], there are two structures: the rhombohedral Th₂Zn₁₇-type structure (space group *R* $\bar{3}m$) and the hexagonal Th₂Ni₁₇-type structure (space group *P6₃/mmc*). Sm₂Co₁₇ and Sm₂Fe₁₇, which have Th₂Zn₁₇-type structures, belong to the *R*₂*T*₁₇ group [6–8]. Not only Sm compounds but also Ce compounds (Ce₂Co₁₇) have been fabricated, and their magnetic anisotropies have been investigated experimentally and theoretically [9,10]. When half of the *R* atoms in *RT*₅ are substituted with *T-T* dumbbells, *RT*₁₂ [(*m*, *n*) = (2, 1)] for the tetragonal ThMn₁₂-type structure (space group *I4/mmm*) can be obtained with the structural change from the orthorhombic structure (space group *Immm*) [11–13]. This group has been studied intensively because it can produce rare-earth-lean and Fe-rich magnets with high magnetization. In particular, it has been found experimentally that nitrogen-intercalated NdFe₁₂ and Sm(Fe,Co)₁₂ films have high magnetocrystalline anisotropies and high remanent magnetizations [14–16], which outperformed the intrinsic magnetic properties of Nd₂Fe₁₄B. In addition to those ordered phases, TbCu₇- or TbCu₉-type structures have been identified as the disordered phase at finite temperatures [17,18]. In this group, the *T-T* dumbbells and *R* atoms are randomly distributed. Because the Sm-Co and Sm-Fe compounds in this group are metastable phases, nonequilibrium processing or third element substitution is necessary to synthesize them [19–22].

The search for other CaCu₅-type derived (meta)stable structures is fundamental and important for developing rare-earth magnets. First-principles calculations based on density functional theory (DFT) is a powerful approach for materials discovery. However, there is an infinite variety in the arrangement of *T-T* dumbbells in CaCu₅-type derived structures, and some structures contain a large number of atoms in a unit cell. This makes direct DFT calculations unsuitable for searching for CaCu₅-type derived structures or disordered TbCu₇-type structures.

*kuroda@ccs.tsukuba.ac.jp

Published by the American Physical Society under the terms of the [Creative Commons Attribution 4.0 International license](https://creativecommons.org/licenses/by/4.0/). Further distribution of this work must maintain attribution to the author(s) and the published article's title, journal citation, and DOI.

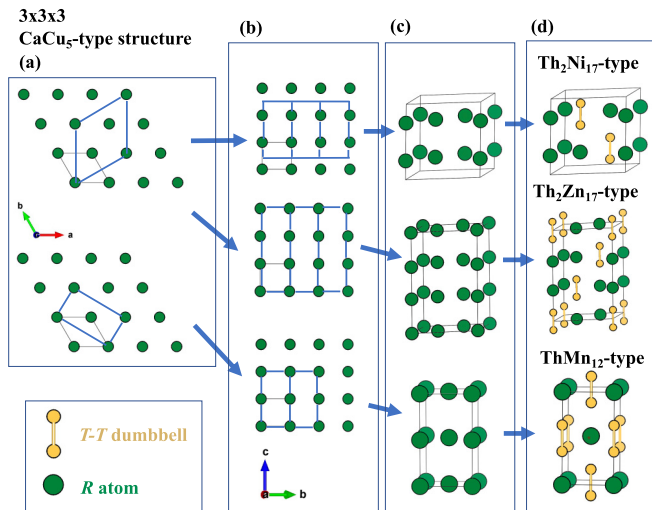


FIG. 1. Structural relation for CaCu_5 -type derived materials. (a) The top view of the $3 \times 3 \times 3$ CaCu_5 -type supercell structure. The unit cell of the corresponding CaCu_5 -type derived structures are plotted with the blue lines. (b),(c) The side view of the $3 \times 3 \times 3$ CaCu_5 -type supercell structure. (d) Some R atoms are replaced by T - T dumbbells, leading to the CaCu_5 -type derived structures.

In this work, we investigate this problem with DFT by using the cluster expansion model (CEM) with DFT data. The CEM has been used to search structures of various materials efficiently and to study order-disorder transitions at finite temperatures [23–25]. We present metastable structure distributions of Sm-Fe and Sm-Co systems and propose other structures that do not exist in available databases with high magnetization. Furthermore, we investigate the formation energies of disordered (TbCu_7 -type) structures and their phase transitions at finite temperatures with the CEM.

II. METHOD

The CEM is constructed as follows. In the CaCu_5 structure, R atoms form a simple hexagonal lattice. Our target structures are generated by replacing some R atoms with T - T dumbbells. By considering the T - T dumbbells as virtual single atoms, we construct the dumbbell CEM, which is written as an Ising-like Hamiltonian,

$$E(\{\sigma\}) = \sum_{\alpha} J_{\alpha} \xi_{\alpha}(\{\sigma\}), \quad (1)$$

$$\xi_{\alpha}(\{\sigma\}) = \frac{1}{N_{\alpha}} \sum_{\{s\}} \sigma_{s_1} \sigma_{s_2} \sigma_{s_3} \dots \sigma_{s_{\alpha}} \quad (2)$$

for the total energies $E(\{\sigma\})$ of the different dumbbell configurations ($\{\sigma\}$). The occupation of the s th site (σ_s) is denoted by pseudospin variables with $\sigma_s = +1$ or -1 for a T - T dumbbell or R atom, respectively. Each dumbbell is placed parallel to the c axis. The J variables are called effective cluster interactions (ECIs) of the clusters (e.g., empty, singlet, pair, and triplet clusters). The singlet cluster represents the concentration of T - T dumbbells ($x = n/m$). The $\xi_{\alpha}(\{\sigma\})$ is the correlation function associated with a cluster specified by α . The sum in Eq. (2) is over all α -tuple clusters. N_{α} is the

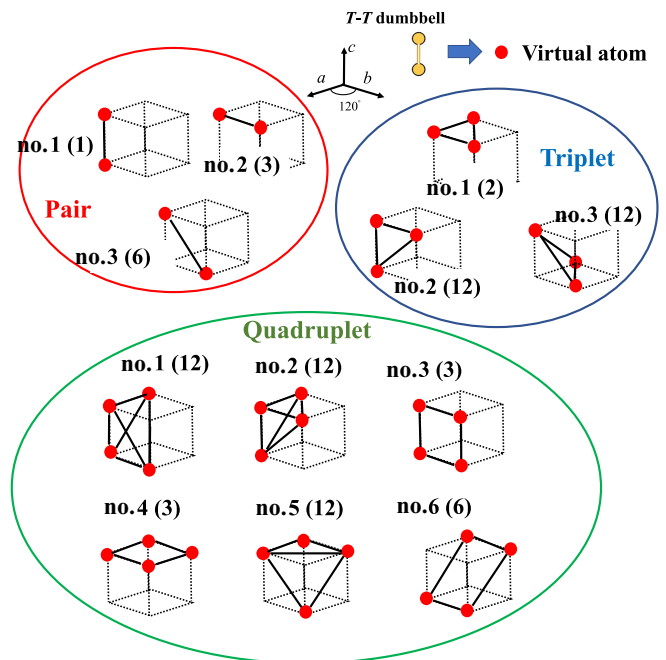


FIG. 2. Clusters considered in our CEM. The numbers in parentheses are the multiplicities (per site). Here the clusters from pairs to quadruplets, except for the empty and singlet clusters, are illustrated.

total number of clusters. These ECIs are determined by the structure inversion method [23] with $E(\{\sigma\})$ obtained from DFT in the generalized gradient approximation [26] using the OPENMX program package [27]. The open-core treatment is used for $4f$ states of Sm atoms [28–30]. For training data, we use the $2 \times 2 \times 2$ supercell of CaCu_5 -type structures and find 22 symmetrically independent structures in this system. These training data do not include the $\text{Th}_2\text{Zn}_{17}$ -type structure, but do include the ThMn_{12} -type structure. Therefore, it is possible to construct the CEM of 22 independent clusters up to octuplets from the 22 structures. However, to avoid the overfitting problem [31], clusters with an order higher than quadruplets are truncated. Thus, we use the CEM with 14 clusters. The selected clusters and these multiplicities are shown in Fig. 2, where the clusters from pairs to quadruplets, except for the empty and singlet clusters, are illustrated. Considering up to quadruplets is necessary to obtain suitable leave-one-out cross-validation (CV) errors for training data (22 structures from the $2 \times 2 \times 2$ supercell). The validation of the obtained CEM and other computational details are explained in the Supplemental Material [3]. These procedures are performed using Python Materials Genomics (Pymatgen) [32] and the Alloy Theory Automated Toolkit (ATAT) program packages [33,34].

III. RESULT

First, we show calculated formation-energy diagrams for the Sm-Fe and Sm-Co systems with respect to the dumbbell concentrations in Fig. 3, and then we discuss the stability of typical ThMn_{12} -type and $\text{Th}_2\text{Zn}_{17}$ -type structures with respect to the ECIs. We search for stable structures by simulated

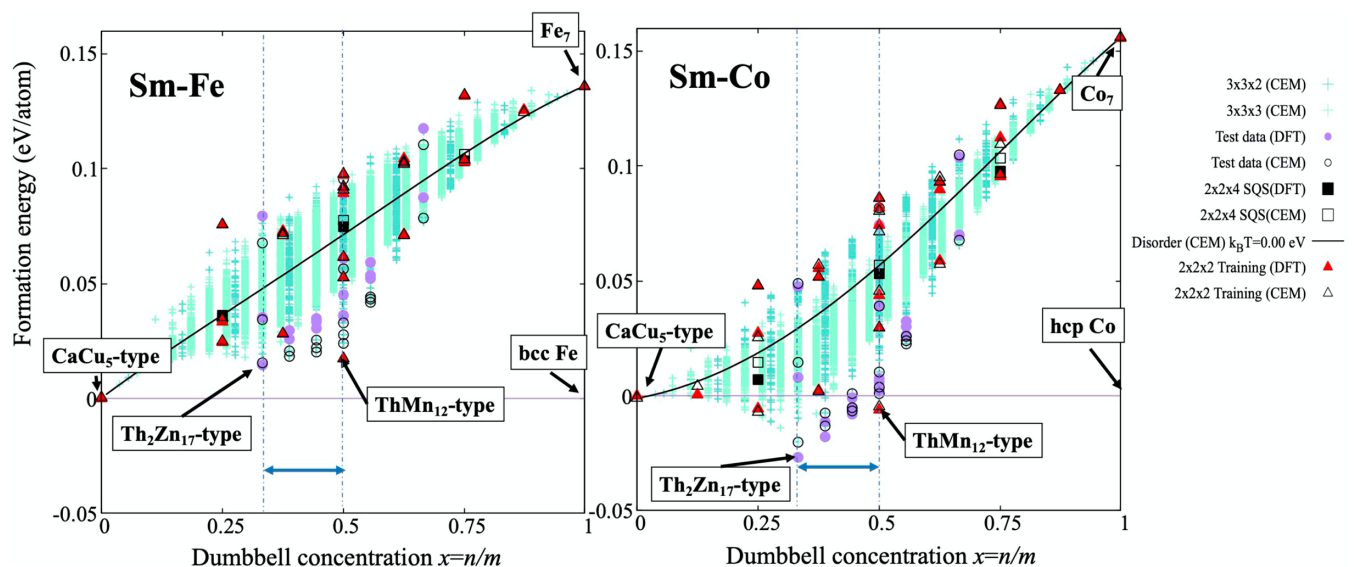


FIG. 3. Calculated formation energies for the Sm-Fe and Sm-Co systems with respect to the dumbbell concentrations. The parent CaCu_5 -type structure (SmFe_5 or SmCo_5) is set to zero at the left side and the most stable simple substance (bcc Fe or hcp Co) is set to zero at the right side for each system. At Fe_7 and Co_7 , the Sm sites are fully filled by the T - T dumbbell. The crosses denote predicted energies in the $3 \times 3 \times 2$ and $3 \times 3 \times 3$ supercells from the CEM. The purple circles, black squares, and red triangles are DFT-calculated energies for the test structures with a $3 \times 3 \times 2$ supercell, special quasirandom structures (SQSs) [35,36], and training structures with a $2 \times 2 \times 2$ supercell, respectively. The corresponding energies calculated by the CEM are shown by the open symbols. The solid lines show the formation energies of disordered (TbCu_7 -type) structures calculated by the CEM.

annealing based on the Monte Carlo method in $3 \times 3 \times 2$ and $3 \times 3 \times 3$ supercells. The crosses in Fig. 3 denote the predicted energies. Among the structure covered by the CEM, the ThMn_{12} -type structure, which has a checkerboardlike structure, is the most stable at $x = 1/2$ in each system (see Fig. S.3 [3]). By considering bcc Fe and hcp Co, the convex hulls are restructured in Fig. 3. This result can be explained by the ECIs for the Sm-Fe and Sm-Co systems in Fig. 4. The labels on the horizontal axis (no. 1, no. 2, ...) correspond to those in Fig. 2. The pair no. 1 clusters have a strong antiferroic (hetero) interaction, introducing the couplings with the Sm atom and T - T dumbbell along the c axes of the CaCu_5 -derived structures (see Fig. 4). Although the pair no. 2 clusters also have an antiferroic interaction, these ECIs are weaker than those of the pair no. 1 clusters. Moreover, because the pair no. 3 clusters have a ferroic (homo) interaction, the T - T dumbbells arranged along the $\langle 101 \rangle$ directions of the hexagonal lattice are energetically preferred.

The $\text{Th}_2\text{Zn}_{17}$ -type structures, which belong to the test data set of the $3 \times 3 \times 3$ supercell, are predicted to be most stable at $x = 1/3$. The stabilities of the $\text{Th}_2\text{Zn}_{17}$ -type structures can be explained mainly by the antiferroic pair no. 1 and no. 2 and ferroic pair no. 3 clusters, which are the same as those of the ThMn_{12} -type structures.

Moreover, the $\text{Th}_2\text{Ni}_{17}$ -type structures are also most stable at $x = 1/3$ in the test data set of the $3 \times 3 \times 2$ supercells for all systems. In the CEM, the $\text{Th}_2\text{Ni}_{17}$ -type structures are energetically degenerate with the $\text{Th}_2\text{Zn}_{17}$ -type structures. In the DFT calculations, the energy difference between the $\text{Th}_2\text{Zn}_{17}$ -type and $\text{Th}_2\text{Ni}_{17}$ -type structures is less than several millielectronvolts per atom, which is smaller than the predicted performance of our model.

Furthermore, $\text{Th}_2\text{Zn}_{17}$ -type $\text{Sm}_2\text{Fe}_{17}$ has a similar formation energy to ThMn_{12} -type SmFe_{12} , and $\text{Th}_2\text{Zn}_{17}$ -type $\text{Sm}_2\text{Co}_{17}$ is more stable than the ThMn_{12} -type SmCo_{12} (see Fig. 3). The ThMn_{12} -type structure has more antiferroic pair no. 1 clusters than the $\text{Th}_2\text{Zn}_{17}$ -type structure, leading

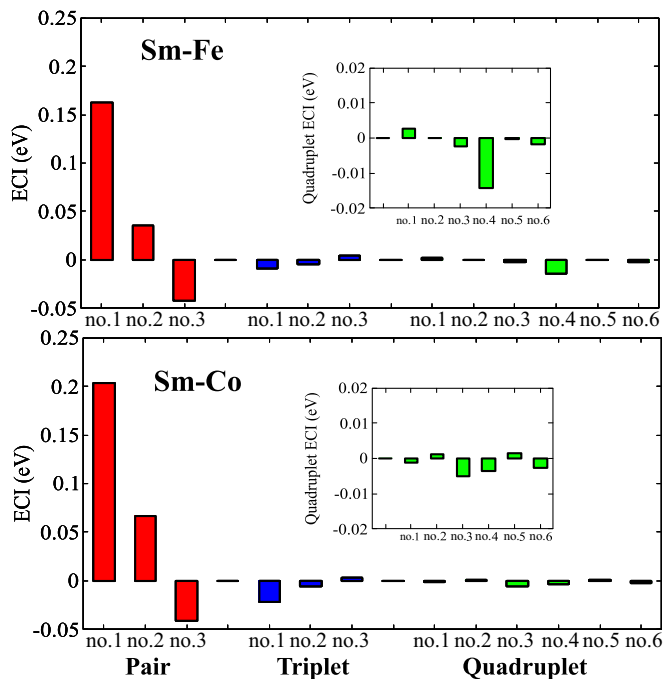


FIG. 4. (a) Calculated ECIs for the Sm-Fe and Sm-Co systems. The numbers following “no.” correspond to the clusters in Fig. 2. The insets are the quadruplet ECIs.

to the stabilization of the ThMn_{12} -type structure. In contrast, the singlet ECI and chemical potentials originating from bcc Fe (hcp Co) and Fe_7 (Co_7) destabilize the Fe or Co-rich composition, resulting in the destabilization of the ThMn_{12} -type structure. Because of this competition and the other ECI, $\text{Th}_2\text{Zn}_{17}$ -type $\text{Sm}_2\text{Co}_{17}$ has a lower formation energy than ThMn_{12} -type SmCo_{12} (see Fig. S.5 [3] for details). Therefore, ThMn_{12} -type SmCo_{12} is predicted to decompose to $\text{Th}_2\text{Zn}_{17}$ -type $\text{Sm}_2\text{Co}_{17}$ and hcp Co.

Some relatively stable structures are concentrated in the $x = 1/3$ and $1/2$ range (Fig. 3). The metastable structures are listed in Fig. S.3 [3]. At concentrations of $x > 1/2$, although more Fe- or Co-rich materials than the ThMn_{12} -type structures are anticipated, our CEM suggests no stable structures in this range. The formation energies rapidly increase with increasing dumbbell concentrations from $x = 1/2$, mainly owing to the pair no. 1 clusters, and all structures in the $x > 1/2$ range have the energetically unfavored T - T dumbbell arrangement along the c axes.

Finally, we discuss the order-disorder transitions of the structures at finite temperatures. The energies of disordered structures are taken from the CEM of the ideal disordered correlation functions of the α -tuple clusters, described as

$$\xi_{\alpha}^{\text{random}} = (1 - 2x)^{\alpha}, \quad (3)$$

where $x (= n/m)$ is the concentration of T - T dumbbells. To consider the free energies ($F = E - TS$) of disordered (TbCu_7 -type) structures including the configurational entropy (S_{config}) at temperature T , we use the Bragg-Williams approximation [23],

$$S_{\text{config}} = k_B \{ (1-x) \ln(1-x) + x \ln x \}, \quad (4)$$

where k_B is the Boltzmann constant. The mean field values for the order-disorder critical temperatures and solubility limits of the T - T dumbbells can be estimated from this one-point approximation. We evaluate the solubility limits of T - T dumbbells in SmT_5 with configuration entropy (see Fig. 5) for the Sm-Fe and Sm-Co systems. The TbCu_7 -type structures become stable as the temperature (T) increases due to the increase of the configurational-entropy term ($-TS_{\text{config}}$) of the free energies. The estimated order-disorder transition of $\text{Th}_2\text{Zn}_{17}$ -type structures for $\text{Sm}_2\text{Fe}_{17}$ and $\text{Sm}_2\text{Co}_{17}$ are at 609 and 1021 K, respectively. This instability of $\text{Sm}_2\text{Fe}_{17}$ may lead to the emergence of the TbCu_7 -type structure experimentally observed [37,38], although the order-disorder transition of $\text{Sm}_2\text{Fe}_{17}$ has not been reported. Because the $\text{Th}_2\text{Zn}_{17}$ -type $\text{Sm}_2\text{Co}_{17}$ has strong pair no. 2 and triplet no. 1 ECIs, the transition temperature of $\text{Th}_2\text{Zn}_{17}$ -type $\text{Sm}_2\text{Co}_{17}$ is significantly higher than that of $\text{Th}_2\text{Zn}_{17}$ -type $\text{Sm}_2\text{Fe}_{17}$ (see Fig. S.5 [3] for details). For the Sm-Co system, the phase transition to the TbCu_7 -type structure occurred around 1573 K in a previous experiment [18], which is about 500 K higher than our estimated value. The vibrational entropy may explain some of the inconsistencies in the TbCu_7 -type phase transition. In the high-temperature region, the vibrational entropy becomes large and can stabilize the ordered $\text{Sm}_2\text{Fe}_{17}$ and $\text{Sm}_2\text{Co}_{17}$ [39].

The estimated solubility limits of the T - T dumbbells may explain the observed composition of experimental TbCu_7 -type structures. According to the experimental results, SmFe_9

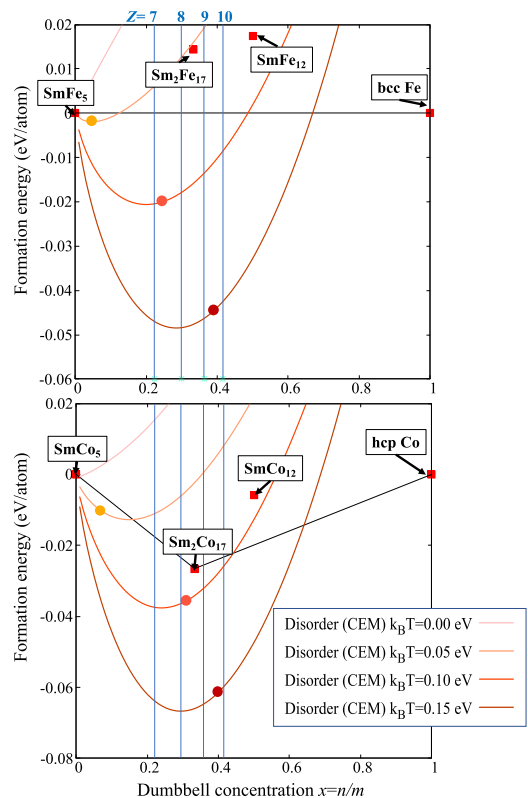


FIG. 5. Formation energies of disordered (TbCu_7 -type) structure calculated by the CEM with configurational entropy. The corresponding solubility limits are shown by the filled circles on the solid lines. The blue vertical lines represent the composition of SmT_Z .

[19] and $\text{SmCo}_{9,8}$ [22] with the TbCu_7 -type structures have been fabricated by using nonequilibrium processing techniques. For $k_B T = 0.15$ eV, which is close to the melting points of Fe and Co, the estimated solubility limits calculated by the CEM are around the SmT_9 compositions.

IV. SUMMARY

In conclusion, by combining DFT with dumbbell CEM, we investigated the structural stabilities of CaCu_5 -type derived materials and predicted metastable structures. The metastable structures are concentrated from $n/m = 1/3$ to $1/2$. Moreover, the configurational entropy of the dumbbell clusters stabilizes the disordered TbCu_7 -type structures at finite temperatures. The estimated solubility-limit of dumbbells are close to the experimental result. However the obtained order-disorder transition temperatures are not in agreement with the experiment. From the previous study about the order-disorder transitions of binary alloys [40], the vibrational entropy is reported to contribute to the transition temperatures. Therefore the effect of vibrational, electronic, and magnetic entropies will be considered in future work.

ACKNOWLEDGMENTS

This work was supported by MEXT via the ‘‘Program for Promoting Researches on the Supercomputer Fugaku’’ (DPMSP) (Grant No. JPMXP1020200307) as part of the

HPCI System Research Project (Project ID: hp200125, hp210179). This work was also partly supported by the Elements Strategy Initiative Center for Magnetic Materials (ESICMM) (Grant No. JPMXP0112101004). The computation was conducted using the facilities of the Supercomputer Center, the Institute for Solid State Physics, The University

of Tokyo, the supercomputer of the Academic Center for Computing, and the supercomputer of the Academic Center for Computing and Media Studies (ACCMS), Kyoto University, the Grand Chariot computational resources provided by Hokkaido University, and the supercomputer Fugaku provided by the RIKEN Center for Computational Science.

-
- [1] M. Sagawa, S. Fujimura, N. Togawa, H. Yamamoto, and Y. Matsuura, *J. Appl. Phys.* **55**, 2083 (1984).
- [2] T. Miyake and H. Akai, *J. Phys. Soc. Jpn.* **87**, 041009 (2018).
- [3] See Supplemental Material at <http://link.aps.org/supplemental/10.1103/PhysRevMaterials.5.124405> for the calculation details and other information.
- [4] G. Hoffer and K. J. Strnat, *J. Appl. Phys.* **38**, 1377 (1967).
- [5] T. Saito and D. Nishio-Hamane, *AIP Adv.* **10**, 015311 (2020).
- [6] J. M. D. Coey and H. Sun, *J. Magn. Magn. Mater.* **87**, L251 (1990).
- [7] K. J. Strnat and R. M. W. Strnat, *J. Magn. Magn. Mater.* **100**, 38 (1991).
- [8] Y. Tawara and H. Senno, *Jpn. J. Appl. Phys.* **14**, 1619 (1975).
- [9] H. Fujii, M. V. Satyanarayana, and W. E. Wallace, *J. Appl. Phys.* **53**, 2371 (1982).
- [10] L. Ke, D. A. Kukusta, and D. D. Johnson, *Phys. Rev. B* **94**, 144429 (2016).
- [11] F. R. De Boer, Y.-K. Huang, D. B. De Mooij, and K. H. J. Buschow, *J. Less-Common Met.* **135**, 199 (1987).
- [12] D. B. De Mooij and K. H. J. Buschow, *J. Less-Common Met.* **136**, 207 (1988).
- [13] K. Ohashi, T. Yokoyama, R. Osugi, and Y. Tawara, *IEEE Trans. Magn.* **23**, 3101 (1987).
- [14] Y. Hirayama, T. Miyake, and K. Hono, *JOM* **67**, 1344 (2015).
- [15] Y. Hirayama, Y. K. Takahashi, S. Hirose, and K. Hono, *Scr. Mater.* **138**, 62 (2017).
- [16] H. Sepehri-Amin, Y. Tamazawa, M. Kambayashi, G. Saito, Y. K. Takahashi, D. Ogawa, T. Ohkubo, S. Hirose, M. Doi, T. Shima, and K. Hono, *Acta Mater.* **194**, 337 (2020).
- [17] K. H. J. Buschow and A. S. van der Goot, *Acta Crystallogr. B* **27**, 1085 (1971).
- [18] Y. Khan, *Acta Crystallogr. B* **29**, 2502 (1973).
- [19] M. Katter, J. Wecker, and L. Schultz, *J. Appl. Phys.* **70**, 3188 (1991).
- [20] Z. X. Zhang, X. Y. Song, W. W. Xu, M. Seyring, and M. Rettenmayr, *Scr. Mater.* **62**, 594 (2010).
- [21] J. Luo, J. K. Liang, Y. Q. Guo, Q. L. Liu, F. S. Liu, Y. Zhang, L. T. Yang, and G. H. Rao, *Intermetallics* **13**, 710 (2005).
- [22] Z. Zhang, X. Song, W. Xu, D. Li, and X. Liu, *J. Appl. Phys.* **110**, 124318 (2011).
- [23] J. W. D. Connolly and A. R. Williams, *Phys. Rev. B* **27**, 5169 (1983).
- [24] K. Terakura, T. Oguchi, T. Mohri, and K. Watanabe, *Phys. Rev. B* **35**, 2169 (1987).
- [25] A. van de Walle and G. Ceder, *J. Phase Equilib.* **23**, 348 (2002).
- [26] J. P. Perdew, K. Burke, and M. Ernzerhof, *Phys. Rev. Lett.* **77**, 3865 (1996).
- [27] T. Ozaki and H. Kino, *Phys. Rev. B* **69**, 195113 (2004).
- [28] M. Richter, *J. Phys. D* **31**, 1017 (1998).
- [29] Y. Harashima, T. Fukazawa, H. Kino, and T. Miyake, *J. Appl. Phys.* **124**, 163902 (2018).
- [30] Y. Tatetsu, Y. Harashima, T. Miyake, and Y. Gohda, *Phys. Rev. Materials* **2**, 074410 (2018).
- [31] N. A. Zarkevich and D. D. Johnson, *Phys. Rev. Lett.* **92**, 255702 (2004).
- [32] S. P. Ong, W. D. Richards, A. Jain, G. Hautier, M. Kocher, S. Cholia, D. Gunter, V. L. Chevrier, K. A. Persson, and G. Ceder, *Comput. Mater. Sci.* **68**, 314 (2013).
- [33] A. van de Walle, M. D. Asta, and G. Ceder, *Calphad* **26**, 539 (2002).
- [34] G. Ghosh, A. van de Walle, and M. Asta, *Acta Mater.* **56**, 3202 (2008).
- [35] A. Zunger, S.-H. Wei, L. G. Ferreira, and J. E. Bernard, *Phys. Rev. Lett.* **65**, 353 (1990).
- [36] A. van de Walle, P. Tiwary, M. M. de Jong, D. L. Olmsted, M. D. Asta, A. Dick, D. Shin, Y. Wang, L.-Q. Chen, and Z.-K. Liu, *Calphad* **42**, 13 (2013).
- [37] T. Saito, F. Watanabe, and D. N.- Hamane, *J. Alloys Compd.* **773**, 1018 (2019).
- [38] T. Tamura and M. Li, *J. Alloys Compd.* **826**, 154010 (2020).
- [39] G. Xing, T. Ishikawa, Y. Miura, T. Miyake, and T. Tadano, *J. Alloys Compd.* **874**, 159754 (2021).
- [40] A. Manzoor, S. Pandey, D. Chakraborty, S. R. Phillpot, and D. S. Aidhy, *npj Comput. Mater.* **4**, 47 (2018).